

Network Calculus Characterization of Congestion Control for Time-Varying Traffic

Harvinder Lehal, Natchanon Luangsomboon, Jörg Liebeherr

Abstract

Models for the dynamics of congestion control generally involve systems of coupled differential equations. Universally, these models assume that traffic sources saturate the maximum transmissions allowed by the congestion control method. This is not suitable for studying congestion control of intermittent but bursty traffic sources. In this paper, we present a characterization of congestion control for arbitrary time-varying traffic that applies to rate-based as well as window-based congestion control. We leverage the capability of network calculus to precisely describe the input-output relationship at network elements for arbitrary source traffic. We show that our characterization can closely track the dynamics of even complex congestion control algorithms.

I. INTRODUCTION

Congestion control in data center networks must deal with highly dynamic workloads with low latency requirements that exchange massive amounts of traffic. A particular difficulty arises from short-lived traffic surges, known as microbursts, that cause periods of high packet delay and loss [1], [2], [3], [4]. Since microbursts occur on a scale below that of a round-trip time, traditional congestion control algorithms (CCAs) are often not well equipped for such scenarios. As a consequence, the quest for effective congestion control in data centers has diverged from congestion control research for long-haul networks [5], [6], [7], [8], [9], [10], [11], [12], [13].

The performance and effectiveness of CCAs for data centers can (and generally is) evaluated in measurement experiments on testbed networks or packet-level simulations. Since measurement studies are tied to the concrete network and protocol settings in which experiments are conducted, generalizations and extrapolations of outcomes can be difficult. A comparable evaluation of CCAs through measurement experiments is not an option when different methods are implemented in different protocol stacks. This is an acute issue in data centers where TCP has been increasingly replaced by RDMA over Converged Ethernet (RoCE) as transport protocol [14], [15]. While some, especially earlier, congestion methods for data centers are integrated into TCP, e.g., DCTCP [6], AC/DC TCP [16], HCC [11], more recent proposals, such as DCQCN [5], Timely [8], HPCC [7], and Swift [9], involve RDMA transport. A performance evaluation of CCAs using a model-based approach can enhance the insights obtained from measurement experiments. A significant benefit of a model-based analysis is the ability to characterize CCAs at a more abstract level, thereby providing a clearer understanding of their operational dynamics and properties. A concern with a model-based analysis of CCAs is the accuracy at which underlying protocols are represented.

The classic model-based analysis approach for CCAs employs a fluid model that expresses network dynamics in terms of a coupled system of delay differential equations [17], [18], [19], [20]. Here, different aspects of a CCA, such as the congestion window, round-trip time, and packet loss rate, are represented as variables, and differential equations describe how the change of one variable affects others. For example, increasing the congestion window leads to higher throughput, but it also increases the likelihood of packet

loss. Fluid models for studying congestion control are well-explored [21] and remain the preferred method for modelling the dynamics of CCAs [5], [22], [23].

While models based on differential equations provide powerful tools for evaluating convergence and stability properties of a CCA, they universally assume that traffic sources are saturated in the sense that they consistently transmit at the maximum rate set by the CCA. Such models are not suitable for evaluating CCAs in traffic scenarios that are susceptible to microbursts, that is, short-lived traffic surges. A notable example of a traffic class exhibiting these characteristics is distributed training of deep neural networks. Here, the traffic of workers involved in the training follows an on-off pattern, where time periods with few transmissions alternate with time periods featuring a sequence of burst transmissions.¹ Even a relatively modest model such as ResNet50 [24] generates up to 10 MB per bursts, with an average transmission rate of 300–400 Mbps per worker in a computation-limited scenario.²

For studying CCAs under intermittent but bursty traffic, we take a different approach, where we describe congestion control algorithms within the framework of the network calculus [25], [26], [27]. Taking advantage of the min-plus convolution operation of the network calculus, we are able to study CCAs for arbitrary time-varying traffic patterns. Our network representation is inspired by the path server model from [28], which takes a network calculus inspired approach for model checking of CCA loss scenarios. We show that a network calculus characterization can closely track the dynamics of even complex congestion control algorithms. In this paper, we make the following key contributions:

- In §III-B, we express events relevant to a CCA, such as acknowledgements, timeouts, retransmissions, congestion notifications, and round-trip times, within the formalism of the network calculus.
- In §III-C and §III-D, respectively, we present models that characterize the dynamics of rate-based and window-based CCAs. By considering time intervals where the network satisfies min-plus linearity and shifting the coordinate system between intervals, we are able to perform a linear analysis of an overall non-linear network system. A comparison with simulations for TCP Vegas [29] evaluates the accuracy of the model.
- In §IV, we address congestion control for flows that share a bottleneck resource. We derive a new network calculus result, which reconstitutes individual traffic flows at the egress of a multiplexer. With this result, we show that our network calculus expression captures convergence toward fairness.
- §V presents a case study of a burst transmission scenario, where we address the interaction between commonly deployed flow control and congestion control methods in data centers with RDMA transport. The case study shows that a network calculus characterization is able to closely track a packet-level simulation.

II. NETWORK CALCULUS BACKGROUND

Network calculus [25], [26], [27] is a methodology for characterizing the input-output relationship of traffic at a network element, where a network element may represent one or a collection of switches, traffic control algorithms, or transmission media. Different from pure fluid flow models, traffic may arrive to and depart from network elements in bursts. As a result, the description of cumulative traffic is not continuous. We describe traffic arriving to and departing from a network element by left-continuous functions A and D , such that $A(t)$ and $D(t)$, respectively, represent the cumulative arrivals and departures at a network element in the interval $[0, t)$, with $D(t) \leq A(t)$. The service at a network element is described

¹The number of bursts relates to the number of convolution layers of the neural network and the burst sizes are determined by the number of parameters within those layers.

²In a computation-limited distributed training scenario, the gradient computation is slower than the communication during gradient reduction.

by another function S , referred to as the element's service curve. Like functions A and D , a service curve S is non-negative and non-decreasing, and we set $A(t) = D(t) = S(t) = 0$ for $t \leq 0$. The backlog at a network element B is a function that describes the traffic arrivals that have not departed, that is, $B(t) = A(t) - D(t)$.

A network element transforms arriving traffic to generate the traffic pattern that departs the network element. With network calculus, the interaction between arriving traffic and a network element is described in terms of a min-plus convolution of the arrival function and the service curve of the network element. The min-plus convolution of two functions f and g , denoted by $f \otimes g$, is defined by $f \otimes g(t) = \inf_{0 \leq s \leq t} \{f(s) + g(t-s)\}$.³ If $D(t) = A \otimes S(t)$ holds for all times t , the service curve S is referred to as an exact service curve. If the inequality $D(t) \geq A \otimes S(t)$ or $D(t) \leq A \otimes S(t)$ holds for all t , we speak of a lower or upper service curve, respectively [25]. An egress port with link rate $r > 0$ can be characterized by an exact service curve $S(t) = \max\{rt, 0\}$, and a token bucket with bucket size $b > 0$ and rate $r > 0$ has an exact service curve $S(t) = \max\{b + rt, 0\}$.

Networked systems that can be described by exact service curves are min-plus linear, in the sense that they are time-invariant and satisfy the superposition principle using the operations of a min-plus dioid algebra [25]. While there exist feedback systems that satisfy min-plus linearity [30], delayed feedback and other factors of congestion control result in a system that is not min-plus linear. In the network calculus, systems that are not min-plus linear can be characterized by lower and upper service curves, however, at a loss of accuracy. In this paper, we maintain a min-plus linear characterization by dividing the time axis into intervals in which the network system satisfies min-plus linearity and characterizing the traffic separately for each interval.

As a remark, the fact that network calculus lends itself to a worst-case analysis of networks (involving lower service curves and upper bounds for arrivals) has invited a misconception that network calculus computations are generally pessimistic. We note that a characterization of min-plus linear systems with exact service curves yields exact quantities for departures, backlog, etc..

We sometimes need to compute the horizontal distance between A and D , or similar functions. If these functions were continuous and strictly increasing, we could compute the horizontal distance between A and D at time t as $t - A^{-1}(D(t))$, where A^{-1} is the inverse function of A with $A^{-1}(A(t)) = t$. However, due to burst arrivals and departures, the functions A and D are not continuous and may have plateaus where no arrivals or departures occur for some time. For these functions, we can compute the horizontal distance using pseudo-inverse functions [31], [32]. For a non-decreasing function F , the upper pseudo-inverse F^\uparrow and lower pseudo-inverse F^\downarrow are defined as

$$F^\uparrow(y) = \sup\{x \mid F(x) \leq y\} \quad \text{and} \quad F^\downarrow(y) = \inf\{x \mid F(x) \leq y\}.$$

With this, the horizontal distance between A and D at time t can be computed with an upper pseudo-inverse as $t - A^\downarrow(D(t))$ or $D^\downarrow(A(t)) - t$, depending on the view point.

III. NETWORK CALCULUS MODEL FOR CONGESTION CONTROL

Our characterization of congestion control techniques exploits that a network that is not min-plus linear may satisfy min-plus linearity within finite intervals. This suggests an iterative approach where we describe the network behavior by an exact service curve for as long as min-plus linearity holds. Then, we establish a new reference system that exploits min-plus linearity in the next time interval.

³With non-continuous functions, we must use infimums and supremums, respectively, instead of minimums and maximums.

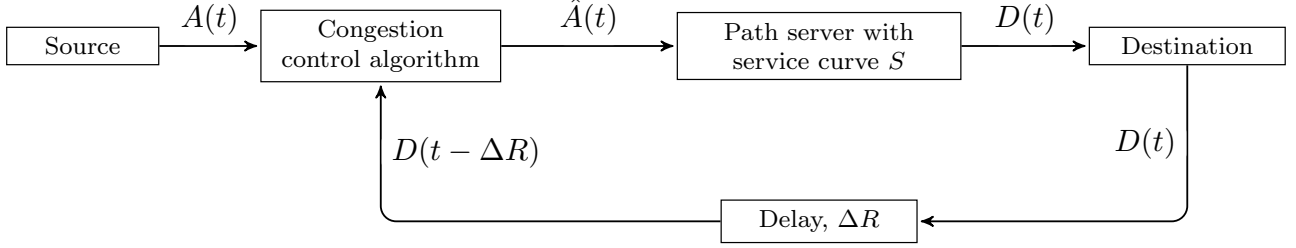


Fig. 1: Path server model with congestion control.

A. Single Flow Model

For a single flow, we resort to the network model shown in Figure 1, which is inspired by the path server model from [28]. We use the following notation for traffic functions:

$A(t)$ –	Arrival function	–	Source traffic generated in the interval $[0, t)$,
$\hat{A}(t)$ –	Admitted arrival function	–	Traffic admitted by a CCA in $[0, t)$,
$D(t)$ –	Departure function	–	Traffic that is received by the destination in $[0, t)$,

with $A(t) \geq \hat{A}(t) \geq D(t)$ for all t . In Figure 1, a source generates traffic according to arrival function $A(t)$. A congestion control algorithm filters the source traffic and admits $\hat{A}(t) \leq A(t)$ into the network. This traffic enters a path server, with exact service curve $S(t)$. The traffic arriving at the destination, $D(t)$, can then be obtained using the min-plus convolution

$$D(t) = \hat{A} \otimes S(t).$$

In the path server model from [28], the network service is described by a token bucket variant, where tokens represent the network capacity available to a traffic flow of interest. In our model, the path server is an arbitrary exact service curve.

B. Modelling Congestion Events

CCAs react to or trigger various congestion events that update the state of the algorithm. We model these signals by analyzing the interaction between arrival and departure functions.

a) Acknowledgments: For each arrival at the destination, we assume that the destination sends acknowledgements back to the source. Assuming, as in the path server model of [28], a fixed delay ΔR , the cumulative acknowledgement function $D(t - \Delta R)$ expresses the arrival of acknowledgments at the source. Assuming that an acknowledgement is issued whenever the equivalent of the maximum packet size I_{\max} has been transmitted, a packet-level version of the acknowledgment function is given by the step function

$$I_{\max} \left\lfloor \frac{D(t - \Delta R)}{I_{\max}} \right\rfloor.$$

b) Timeouts: Packet timeouts are used by some CCAs to indicate that the network is facing congestion and that the transmission rate should be lowered. In TCP, this is referred to as an RTO timeout [33]. Let τ_o represent the maximum duration that a packet can be unacknowledged. To simplify the analysis, we assume that τ_o is a constant. We can represent the least amount of traffic that should be acknowledged by time t as $\hat{A}(t - \tau_o)$, and refer to it as the *timeout function*. A timeout occurs at time t , when the acknowledgements function falls below the timeout function, that is,

$$D(t - \Delta R) < \hat{A}(t - \tau_o).$$

c) *Retransmissions*: Timeout congestion events may result in retransmissions of data, generally by resuming transmissions starting at the data that triggered a timeout (Go-Back-N). Since traffic functions for arrivals and departures in the network calculus are assumed to be non-decreasing, retransmissions do not fit easily into the framework. In our analysis, this is addressed through a shift of the coordinate system, whereby the origin is moved to the coordinates of the first retransmission. The details of this technique are given in §III-C.

d) *Explicit Congestion Notification (ECN)*: ECN [34] is a method for signaling network congestion before a packet loss has occurred. When the backlog at a switch buffer exceeds a threshold K_{\max} , packets are marked with a congestion signal. When such a signal arrives at the destination, a congestion notification is sent back to the source, which then reduces its transmissions. ECN methods often incorporate Random Early Drop (RED) [35], which adds a second buffer threshold K_{\min} ($K_{\min} < K_{\max}$) and a probability P_{\max} ($0 < P_{\max} \leq 1$), and marks packets that encounter a backlog of x with probability $p(x)$ given by

$$p(x) = \begin{cases} 1, & \text{if } x \geq K_{\max}, \\ P_{\max} \frac{x - K_{\min}}{K_{\max} - K_{\min}}, & \text{if } K_{\min} < x < K_{\max}, \\ 0, & \text{if } x \leq K_{\min}. \end{cases}$$

CCAs generally issue or react to congestion events at most once per round-trip time. This can be enforced either through timers, as in DCQCN [5] or by counting bytes as in TCP [34].

We describe an ECN variant that specifies a minimum time interval $\Delta\tau_{\text{ecn}}$ between congestion notifications. In the single flow model, the backlog, B , in the path server at time t is given by

$$B(t) = \hat{A}(t) - D(t),$$

and a packet is marked at time t if $B(t) \geq K_{\max}$. We assume that congestion notifications can be triggered by a destination as soon as the packet is marked. Every notification arrives at the source with a fixed latency ΔR .

Suppose a packet is marked at time t ($B(t) \geq K_{\max}$). Let \underline{t} denote the transmission time of the most recent notification before t or, in case a notification has been scheduled for a time after time t , the next notification after time t . There are three cases to consider:

- 1) $t - \underline{t} \geq \Delta\tau_{\text{ecn}}$: In this case, the notification can be sent immediately at time t , and we set $\underline{t} = t$.
- 2) $0 \leq t - \underline{t} < \Delta\tau_{\text{ecn}}$: In this case, the next notification is sent at $\underline{t} + \Delta\tau_{\text{ecn}}$, and we set $\underline{t} = \underline{t} + \Delta\tau_{\text{ecn}}$.
- 3) $t - \underline{t} < 0$: Here a notification has already been scheduled in the future, and no action needs to be taken.

To make sure that the first time t with $B(t) \geq K_{\max}$ triggers a congestion notification, we initially set $\underline{t} = -\infty$. To account for RED, the marking of traffic must additionally consider backlog in the range $[K_{\min}, K_{\max})$ where traffic is marked according to the above probability function.

e) *Priority Flow Control (PFC)*: Specified in [36], PFC is a link-level flow control mechanism between two switches or between a switch and a host. PFC seeks to achieve a lossless service by stopping arrivals from upstream switches or hosts. The endpoints of a link are designated as sender or receiver. A backlog exceeding threshold X_{off} at an ingress port of a receiver indicates that a link is congested. In this case, the receiver temporarily stops additional arrivals from the sender by sending it a *Pause* packet. By pausing transmissions sufficiently early, buffer overflows at the receiver can be fully prevented. Transmissions by the sender are paused until the backlog at the receiver reaches X_{on} ($X_{\text{on}} < X_{\text{off}}$). Assuming again a constant delay ΔR for the *Pause* packet in the path server model, the next time after time t when transmissions are paused, is given by

$$t_P(t) = \inf\{s \geq t \mid B(s - \Delta R) > X_{\text{off}}\}.$$

Assuming a line rate of C , transmissions can resume at

$$t_R(t) = t_P(t) + \frac{X_{\text{off}} - X_{\text{on}}}{C}.$$

f) Round-trip Time (RTT): The round-trip time (RTT) refers to the total time it takes for a packet to travel from a source to a destination and back again. Some congestion control algorithms such as TCP Vegas [29] and Timely [8] use measurements of the RTT to infer whether congestion is growing or receding. In the path server model, the RTT is represented by the variable one-way delay from the source to the destination plus the constant delay ΔR . The one-way delay through the path server is represented by the horizontal distance between the departure function D and the admitted arrival function \hat{A} . For the RTT measured at time t , denoted by $\text{RTT}(t)$, we account for the delay ΔR by considering the horizontal distance at time $t - \Delta R$. Using pseudo-inverse functions, $\text{RTT}(t)$ can be expressed as

$$\begin{aligned} \text{RTT}(t) &= ((t - \Delta R) - \hat{A}^\downarrow(D(t - \Delta R)) + \Delta R \\ &= t - \hat{A}^\downarrow(D(t - \Delta R)). \end{aligned} \quad (1)$$

C. Rate-Based Congestion Control

We next consider a rate-based CCA that sets the maximum transmission rate of the source. Since the rate is piecewise constant over two congestion events, we can describe the CCA rate limit by an exact service curve of $S_r = \max(rt, 0)$, where the rate r changes according to congestion signals. Assuming that the rate is initialized to r_o , we therefore obtain

$$\hat{A}(t) = A \otimes S_{r_o}(t) \quad \text{and} \quad D(t) = \hat{A} \otimes S(t). \quad (2)$$

We consider a CCA that applies an Additive-Increase-Multiplicative-Decrease (AIMD) algorithm [37] and uses a timeout as an indicator of congestion. Recall that a timeout event occurs when the acknowledgement function $D(t - \Delta R)$ falls below the timeout function $\hat{A}(t - \tau_o)$. In this case the rate is decreased proportionally by

$$r(t) = \beta \cdot r(t^-), \quad (3)$$

where $0 < \beta < 1$ is a constant. Here we use the notation $r(t^-)$ to indicate the rate just before the timeout occurred. An additive increase of the rate is achieved by allowing a rate increase only after a fixed time interval, which we denote by $\Delta\tau_{\text{ai}}$. A rate increase occurs only if there was no timeout and no congestion notification in the previous interval, that is, for all $s \in [t, t - \Delta\tau_{\text{ai}}]$, $D(s - \Delta R) \geq \hat{A}(s - \tau_o)$ and $s - \Delta R$ does not satisfy the conditions for sending a congestion notification as described in §III-B. The rate is increased by an additive constant $\alpha > 0$ by

$$r(t) = r(t^-) + \alpha. \quad (4)$$

When the CCA updates the rate limit $r(t)$, the service curve S_r changes, and the convolution expressions in Eq. (2) are no longer valid. By resetting the coordinate system and revising function \hat{A} , we can obtain a new min-plus linear system and continue the computation of the departure function D .

We next illustrate the shift of the coordinate system for a timeout event and the subsequent retransmissions. Consider the scenario in Figure 2a, which has an arrival function $A(t)$ that is rate-limited to yield an admitted function \hat{A} . The departures from the path server are described by $D(t)$. At time t_{TO} , the timeout function $\hat{A}(t - \Delta R)$ becomes larger than the acknowledgement function $D(t - \Delta R)$, indicating a timeout event. At this time, the CCA updates the rate limit according to Eq. (3).

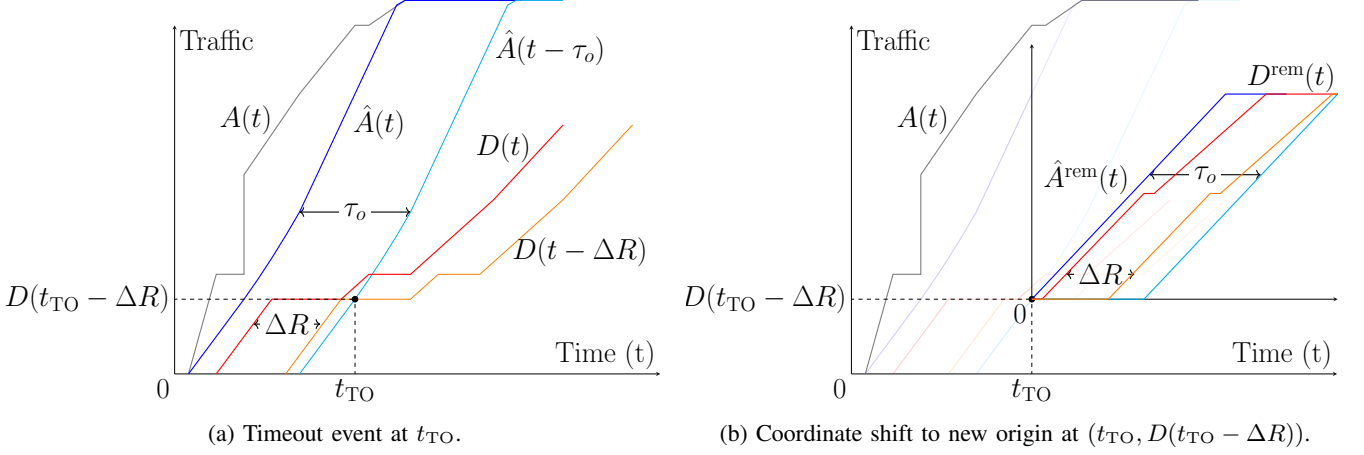


Fig. 2: Updating the rate-based traffic functions after a timeout event. (Arrival function $A(t)$ in gray, admitted arrival function \hat{A} in blue, departure function $D(t)$ in red, timeout function $\hat{A}(t - \Delta R)$ in cyan, acknowledgement function $D(t - \Delta R)$ in orange).

The sender knows at time t_{TO} that an amount given by $D(t_{TO} - \Delta R)$ has been successfully delivered. Assuming a Go-Back-N scheme, the remaining unacknowledged packets, $\hat{A}(t_{TO}) - D(t_{TO} - \Delta R)$, need to be retransmitted. As a result, \hat{A} is no longer a non-decreasing function and the min-plus convolution operation is no longer applicable. Additionally, after the timeout event, the rate limit is reduced according to Eq. (2) and the service curve of the CCA becomes $S_{r(t_{TO})} = \max\{r(t_{TO})t, 0\}$.

The retransmission as well as the multiplicative decrease of the rate limit can be captured through a change of the coordinate system, where we move the origin to coordinates $(t_{TO}, D(t_{TO} - \Delta R))$. This is shown in Figure 2b. In the new coordinate system, the traffic functions are given the superscript 'rem' to indicate that they represent the remaining traffic. We set $A^{rem}(t) = \hat{A}^{rem}(t) = D^{rem}(t) = 0$ for $t \leq 0$. The new arrival function A^{rem} corresponds to the traffic that has not been transmitted or been not acknowledged by time t_{TO} , yielding

$$A^{rem}(t) = A(t + t_{TO}) - D(t_{TO} - \Delta R).$$

Note that the function has an initial burst $A(t) - D(t_{TO} - \Delta R)$. Since the modified arrival function is non-decreasing we can apply the min-plus convolutions to obtain the admitted arrival and departure functions by

$$\begin{aligned}\hat{A}^{rem}(t) &= A^{rem} \otimes S_{r(t_{TO})}(t), \\ D^{rem}(t) &= \hat{A}^{rem} \otimes S(t).\end{aligned}$$

These functions can be used to update the original functions for times $t \geq t_{TO}$ by

$$\begin{aligned}\hat{A}(t) &= \hat{A}^{rem}(t - t_{TO}) + D(t_{TO} - \Delta R), \\ D(t) &= D^{rem}(t - t_{TO}) + D(t_{TO} - \Delta R).\end{aligned}$$

A similar coordinate shift and update is performed whenever the rate limit is increased. For each time t_{AI} where an additive increase according to Eq. (4) occurs we reset the origin to $(t_{AI}, \hat{A}(t_{AI}))$, which indicates the amount of traffic that has been admitted to the network so far. Here, the modified arrival function A^{rem} becomes

$$A^{rem}(t) = A(t + t_{AI}) - \hat{A}(t_{AI}).$$

After updating the rate limit to $r(t_{AI})$, the admitted arrivals and departures are computed with the min-plus convolution as shown above. The computations for the rate-based congestion control are summarized in an algorithm in Appendix A.

D. Window-Based Congestion Control

With window-based congestion control, the CCA limits the total number of bytes that can have outstanding acknowledgements, the so-called congestion window. The majority of CCAs for TCP, from Tahoe [38] to CUBIC [39], follow a window-based approach. A major difference between rate-based and window-based CCAs is that the latter allows back-to-back transmissions, which increases the burstiness of traffic. Here, we model a basic window-based CCA with AIMD, similar to Reno [33] for the path server model from Figure 1.

Let W denote the size of the congestion window, the exact service curve associated with window-based congestion control is given by

$$S_W(t) = \begin{cases} 0, & \text{if } t \leq 0, \\ W, & \text{if } t > 0. \end{cases}$$

With this service curve, the admitted arrival and departure functions are computed as

$$\hat{A}(t) = A \otimes S_W(t) \quad \text{and} \quad D(t) = \hat{A} \otimes S(t). \quad (5)$$

In practice, window-based CCAs update W each time an acknowledgement of previously unacknowledged data is received. In our characterization, we update the congestion window only after W bytes have been acknowledged. The amount of data corresponding to W is referred to as a *flight*. Starting with an initial congestion window W_o , the transmission of the initial flight is completed at t_W given by

$$t_W = \inf \{t > 0 \mid D(t - \Delta R) \geq W_o\}.$$

With an additive increase, after the transmission of a flight, the congestion window is increased by a constant $\alpha > 0$, that is,

$$W = W_o + \alpha. \quad (6)$$

After a timeout, that is, a time t_{TO} with $D(t_{TO} - \Delta R) < \hat{A}(t_{TO} - \tau_o)$, the congestion window is reduced by a multiplicative factor β ($0 < \beta < 1$), that is, $W = \beta W_o$.

Whenever the congestion window is updated according to Eq. (6), we perform a shift of the coordinate system. After the transmission of a flight, the origin of the coordinate system is set to $(t_W, \hat{A}(t_W))$. After a timeout at some time t_{TO} , the coordinate system is adjusted as described in §III-C with a new origin $(t_{TO}, D(t_{TO} - \Delta R))$. In both cases, due to resetting the origin, the updated congestion window becomes the initial window size, that is, $W_o = W$. The remaining traffic functions A_{rem} , \hat{A}_{rem} , and D_{rem} in the new coordinate system are constructed as described in §III-C.

Some CCAs use a multiplicative increase when the window size is below a value $w_{th} < W$. In TCP Tahoe, Reno, and its variants, the value is referred to as slow start threshold, and a time period of a multiplicative increase is referred to as a slow start phase. Typically, W is doubled after a flight, resulting in an update

$$W = \begin{cases} 2W, & \text{if } W < w_{th}, \\ W + a, & \text{if } W \geq w_{th}. \end{cases} \quad (7)$$

After a timeout event, the slow start threshold is reduced by a multiplicative factor ($w_{th} = \beta W$) and the congestion window is reduced to one packet with maximal length. Appendix B presents an algorithm for the network calculus computations for window-based congestion control.

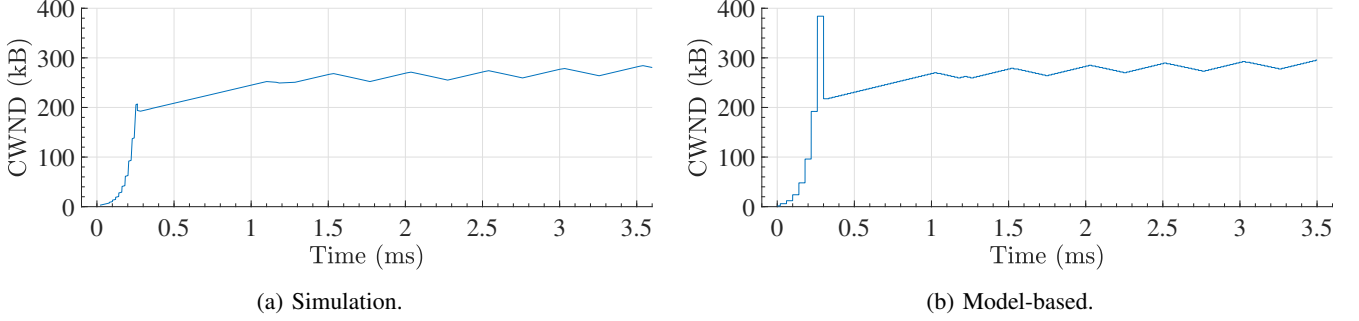


Fig. 3: Congestion window (CWND) of TCP Vegas.

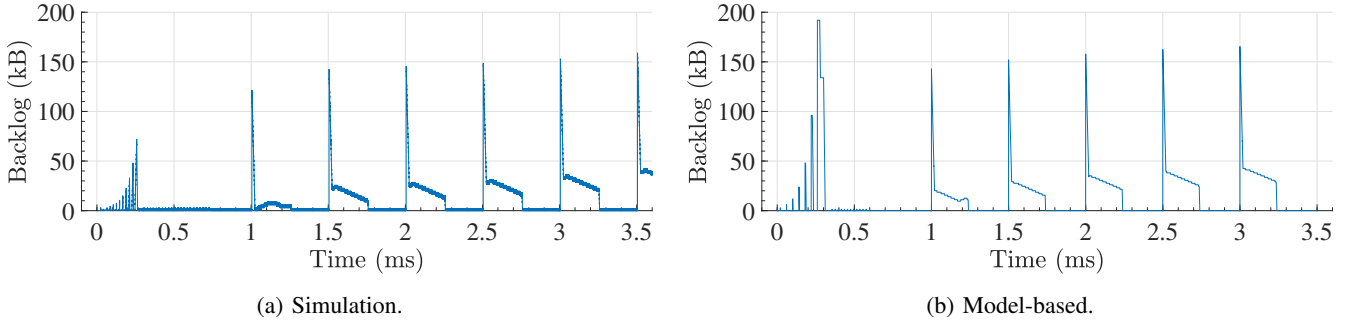


Fig. 4: Backlog produced by TCP Vegas with our traffic scenario.

E. Example: TCP Vegas

To evaluate how well CCA dynamics are captured by our network calculus model, we compare a model-based characterization of TCP Vegas [29] with a packet-level simulation. TCP Vegas is a window-based CCA that uses RTT estimates for updating its congestion window with the goal of keeping the backlog within a specified range. It has a slow-start phase, which doubles the congestion window every other round-trip time.

We consider a bursty transmission scenario of a single traffic source at a 100 Gbps link, which initially issues a 4 MB burst and then transmits at fixed rate of 50 Gbps. Additionally, starting at $t = 1$ ms, the source issues instantaneous bursts of 1.5 MB every 0.5 ms. Each of the bursts creates a backlog at the link.

For the simulations, we use the TCP Vegas implementation included in the ns-3 distribution [40] and set protocol parameters as in [41]. The network topology consists of the source, a switch, and a destination node. Links have a propagation delay of $5 \mu s$, resulting in a round-trip delay between the source and the destination of $20 \mu s$. Figures 3a and 4a, respectively, present the congestion window at the source and the backlog at the switch.

Our model-based characterization uses a path server with fixed rate of $C = 100$ Gbps and feedback delay $\Delta R = 20 \mu s$. The computations in §III-D are modified to account for RTT measurements and different congestion window updates. Appendix C presents an algorithm of the calculations for TCP Vegas. Figures 3b and 4b depict the congestion window and the backlog computed by the model.

There are two deviations between the simulation and the network calculus model. The first difference concerns the *baseRTT* parameter. The simulation sets it to the smallest RTT measurement since the connection started, whereas the model sets it to the feedback delay ΔR . The second difference relates to

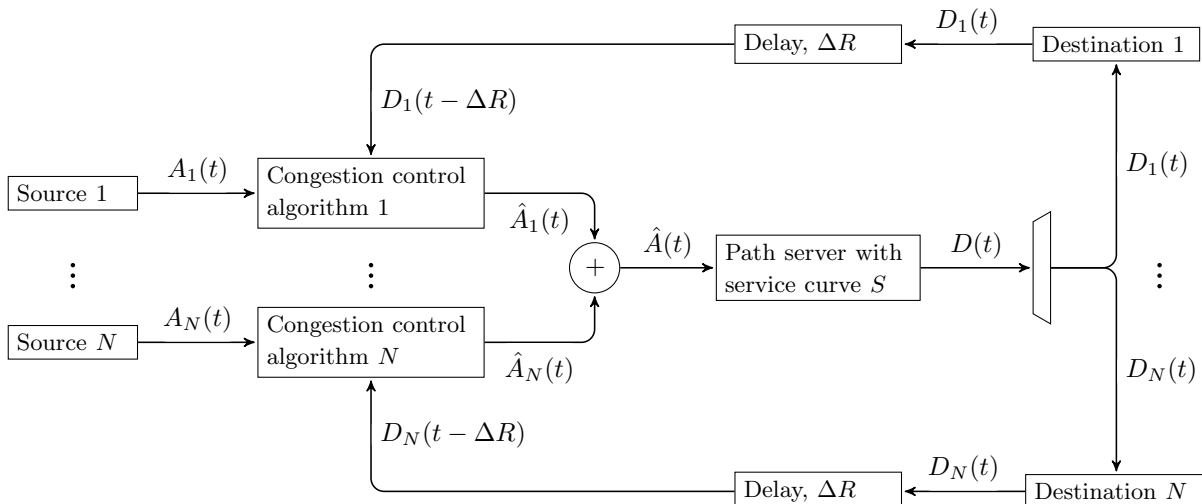


Fig. 5: Multi-flow model for congestion control.

the window increases during the slow start phase. The ns-3 simulation updates the window for each new acknowledgement, whereas our model follows the TCP Vegas specification in [41], [29] and doubles the window for every two RTT updates.

A comparison of Figures 3 and 4 shows that the model-based characterization closely matches the simulation. The largest deviation, observed in the interval $[0, 0.5]$ ms, is due to the different window updates during the slow start phase. Beyond this, the model captures the variations and trends of the congestion window during burst arrivals.

IV. MULTI-FLOW ANALYSIS

To study fairness properties of CCAs we must extend the path server model from Figure 1 to accommodate multiple flows. The extended model is shown in Figure 5, where multiple traffic sources that are each regulated by a CCA are multiplexed at the path server resulting in the admitted arrival function $\hat{A}(t) = \sum_{j=1}^N \hat{A}_j(t)$. At the egress of the path server, the departure traffic D is demultiplexed into per-flow departure functions D_j , which are then used for the acknowledgement functions. For simplicity, we assume that the feedback delay ΔR is identical for all flows.

Obtaining expressions for D_j is challenging, since it depends on the operation of the path server, in particular, how the path server schedules traffic from different flows. In the next subsection, we present a derivation of D_j for a path server with FIFO multiplexing. Obtaining expressions for D_j under priority or fair queuing involves less effort.

A. Demultiplexing Departures at a FIFO Element

Consider a path server as shown in Figure 5, which sees arrivals from a set $\mathcal{N} = \{1, \dots, N\}$ of flows, and which transmits traffic in FIFO order. Since, with FIFO, traffic departs in the order of its arrival, if at some time t the traffic of a flow that arrived before time $t' \leq t$ departs, it also holds for every other flow. We call this the *FIFO property*.

Definition 1. (FIFO property) A path server that sees arrivals from a set of flows \mathcal{N} has the FIFO property if, for every $i, j \in \mathcal{N}$ and every time interval $[t', t]$,

$$\hat{A}_i(t') < D_i(t) \implies \hat{A}_j(t') \leq D_j(t). \quad (8)$$

The strict inequality on the left-hand side of Eq. (8) is needed to account for simultaneous packet arrivals. Note that in FIFO, the order of departures between simultaneous arrivals is arbitrary. If the arrival function is continuous or if simultaneous packet arrivals from multiple flows can be excluded, the strict inequality can be relaxed to allow for equality.

The following lemma shows that the FIFO property can be extended to an aggregation of flows. The proof of the lemma as well as other proofs in this section are given in Appendix D.

Lemma 1. *Given a path server with \mathcal{N} flows that satisfies the FIFO property. For any subset $X \subseteq \mathcal{N}$ and any flow $i \in \mathcal{N}$, every time interval $[t', t]$ satisfies*

$$\hat{A}_i(t') < D_i(t) \implies \sum_{j \in X} \hat{A}_j(t') \leq \sum_{j \in X} D_j(t), \text{ and} \quad (9)$$

$$\sum_{j \in X} \hat{A}_j(t') < \sum_{j \in X} D_j(t) \implies \hat{A}_i(t') \leq D_i(t). \quad (10)$$

Similar to Eq. (8), if the arrival function is continuous, or if there are no simultaneous packet arrivals from different flows, the left equations of Eq. (9) and (10) can be relaxed to allow for equality. Then, the implications in the lemma can be combined into

$$\hat{A}_i(t') \leq D_i(t) \iff \sum_{j \in X} \hat{A}_j(t') \leq \sum_{j \in X} D_j(t).$$

If the aggregate arrival and departure functions $\sum_{j \in X} \hat{A}_j(t')$ and $\sum_{j \in X} D_j(t)$ coincide for two times t' and t with $t' < t$, we can calculate the departure function of individual flows.

Lemma 2. *Given a buffer with \mathcal{N} flows that satisfies the FIFO property. For any subset $X \subseteq \mathcal{N}$ and every time interval $[t', t]$, if*

$$\sum_{j \in X} \hat{A}_j(t') = \sum_{j \in X} D_j(t), \quad (11)$$

then for any flow $i \in \mathcal{X}$,

$$\hat{A}_i(t') = D_i(t). \quad (12)$$

Using Lemmas 1 and 2, we can calculate the bounds of the departure function of individual flows from a FIFO buffer.

Theorem 1. *Let \mathcal{N} be a set of flows at a buffer that satisfies the FIFO property. Then the departure function of every flow $i \in \mathcal{N}$ is bounded for arbitrary $\varepsilon > 0$ by*

$$\hat{A}_i(\hat{A}^\dagger(D(t))) \leq D_i(t) \leq \hat{A}_i(\hat{A}^\dagger(D(t)) + \varepsilon).$$

If \hat{A}_i is continuous, the upper bound in Theorem 1 reduces to the lower bound for $\varepsilon \rightarrow 0$, and the value of $D_i(t)$ can be computed exactly.

B. Example: AIMD Fairness

With §IV-A we can analyze the dynamics of congestion control for concurrent flows. We now present an example that evaluates how well the model-based network calculus characterization tracks a convergence of a CCA to a fair allocation. We consider a scenario with two flows that each deploy a rate-based AIMD algorithm as in §III-C with $\alpha = 100$ Mbps and $\beta = 0.8$. The time interval between rate increases is $\Delta\tau_{ai} = 30 \mu\text{s}$. The feedback delay is set to $\Delta R = 20 \mu\text{s}$ and the timeout value is $\tau_o = 100 \mu\text{s}$. The

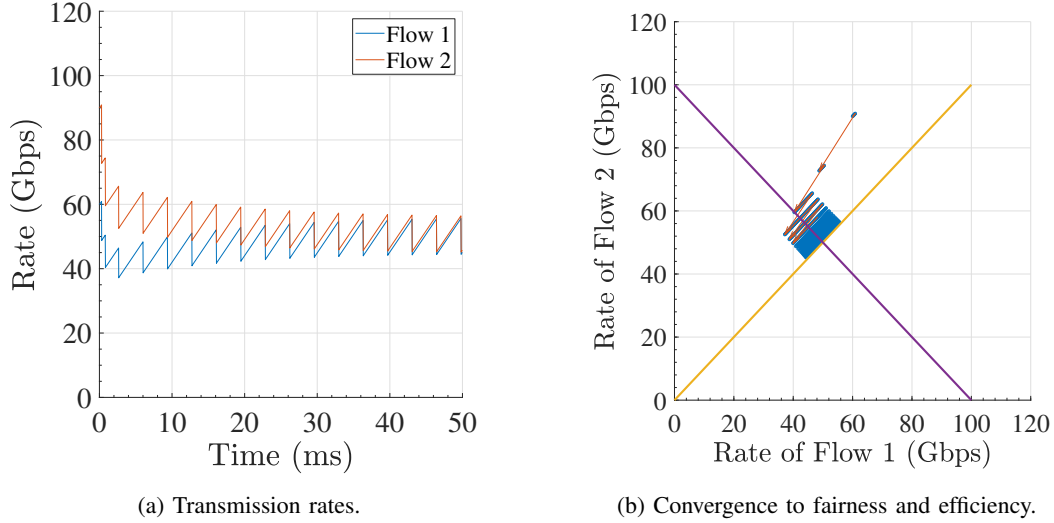


Fig. 6: Fairness at a FIFO path server.

path server is assumed to have an exact service curve $S(t) = \max\{Ct, 0\}$ with $C = 100$ Gbps. There are two flows that start transmissions with rates 60 Gbps and 90 Gbps.

The computations apply Algorithm 1 based on the derivations in §III-C. Figure 6a shows the rates of the two flows over a time period of 50 ms. Figure 6b depicts a vector representation of the rates as suggested in [37]. The figure includes two lines: a fairness line (yellow) where both flows are allocated the same rate, and an efficiency line (purple) where both flows consume all link resources. The intersection of the two line is the optimal operating point. Starting at the initial point (60, 90), the shown graph shows the convergence to the optimal operating point using a quiver plot. Clearly, the model-based characterization is able to capture the convergence to a fair resource allocation.

V. CASE STUDY: DATA CENTER CONGESTION CONTROL

In this section we consider a congestion control scenario in a data center network, where we compare a packet-level simulation with our network calculus analysis. We consider a data center network with RDMA transport over RoCEv2, which performs RDMA with UDP encapsulation [15]. RoCEv2 networks support a lossless Ethernet service which is realized with the PFC protocol (see §III-B). The de-facto standard for congestion control in these networks is Data Center Quantized Congestion Notification (DCQCN) [5], which is supported by numerous vendors [42], [43], [44], [45]. Unless PFC is disabled, it runs in conjunction with DCQCN.

At its core, DCQCN is a rate-based CCA with ECN and RED for congestion notifications. DCQCN overall follows an AIMD approach for setting the transmission rates of senders. Congestion notification packets (CNPs) sent to senders must be separated by a gap of at least T_{gap} . In detail, the rate adjustment at the senders is as follows:

- A sender maintains two rate limits R_C and R_T . Upon receiving a CNP the limits are updated by $R_T = R_C$, $R_C = (1 - \alpha)R_C$, and $\alpha = \alpha + g(1 - \alpha)$, where $\alpha \in [0, 1]$ is a rate reduction factor, which itself is tuned by a parameter $g \in [0, 1]$. Initially, R_T and R_C are set to the line rates, and α is set to 1.
- When a time K has elapsed since the last CNP arrival, the sender sets $\alpha = (1 - g)\alpha$.
- Every T time units without receiving a CNP, a counter i_T is increased by 1, and for every B bytes transmitted without receiving a CNP, i_B is increased by 1. After 5 increments of i_T or i_B , the

TABLE I: Increase of transmission rates in DCQCN.

Phase	Condition	Changes
Fast recovery	$\max\{i_T, i_B\} < 5$	R_T unchanged, $R_C = (R_C + R_T)/2$
Additive increase	$\max\{i_T, i_B\} \geq 5$	$R_T = R_T + R_{AI}$, $R_C = (R_C + R_T)/2$
Hyper increase	$\min\{i_T, i_B\} \geq 5$	$R_T = R_T + (\min\{i_T, i_B\} - 5)R_{HI}$ $R_C = (R_C + R_T)/2$

TABLE II: Parameter setting for DCQCN from [5], [46].

K_{\min}	K_{\max}	P_{\max}	g	T_{gap}	K, T	B	R_{AI}	R_{HI}
5 kB	200 kB	1%	1/256	50 μs	55 μs	10 MB	5 Mbps	50 Mbps

sender updates the transmission rates R_C and R_T using the additive constants R_{AI} and R_{HI} . The rate increases of R_C and R_T depend on the current values of i_T or i_B and are as given in Table I. Whenever a sender receives a CNP, it sets $i_B = i_T = 0$.

Table II lists parameter values for DCQCN for a DCN switch as suggested in [5], [46]. For PFC we set $X_{\text{off}} = 9.5$ kB/port/Gbps and $X_{\text{on}} = 9.25$ kB/port/Gbps.

a) Transmission scenario.: We consider a transmission scenario that may occur during distributed training of deep neural networks, when multiple workers concurrently transmit gradients of model parameters through the same output port of a switch. We consider a shared memory switch with 32 ports that operate at 100 Gbps. Each port is connected to a host, of which 31 hosts are traffic senders and one host is the destination for all traffic. The propagation delay of links between hosts and the switch is set to 1 μs . The switch memory is assumed to be large enough so that buffer overflows do not occur. We consider a scenario where all traffic senders start the transmission of a burst with size 10 MB, which corresponds to the parameter size of the largest convolution layer in ResNet50 [24]. We consider three network configurations:

<i>PFC</i>	–	PFC is enabled, DCQCN is not enabled,
<i>DCQCN</i>	–	DCQCN and PFC are enabled,
<i>DCQCN-noPFC</i>	–	DCQCN is enabled, PFC is not enabled.

A. Packet-level Simulation Results

We perform simulations using a publicly available ns-3 simulation for DCQCN and PFC over RoCEv2 [47]. Figure 7a shows the aggregate traffic arrival rate at the switch for a duration of 10 ms, starting at $t = 1000$ ms, where rates are computed as averages over 1 μs , and Figure 7b shows the resulting backlog at the switch.

The transmission rates for *PFC* in Figure 7a (shown in green color) exhibit an on-off behavior. Since the aggregate traffic to the port with the destination host exceeds its link rate, backlog accumulates at the switch. When the threshold X_{off} is reached, arrivals are stopped until the backlog falls below X_{on} . Since all senders start transmissions at the same time, the pause and resume events are synchronized, which creates the observed periodic traffic pattern. The resulting backlog for *PFC* seen in Figure 7b shows that the backlog initially builds up to around 30 MB and then stays at a high level.

The results for *DCQCN* and *DCQCN-noPFC*, respectively, are shown as blue and red curves in Figure 7. Initially, the traffic rates are high for both configurations, since DCQCN sets the initial transmission rates

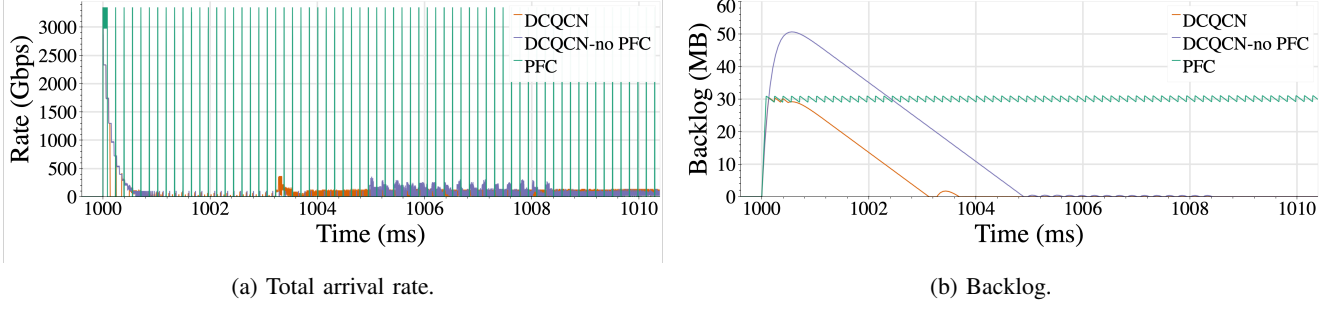


Fig. 7: Simulation of burst arrivals (10 ms).

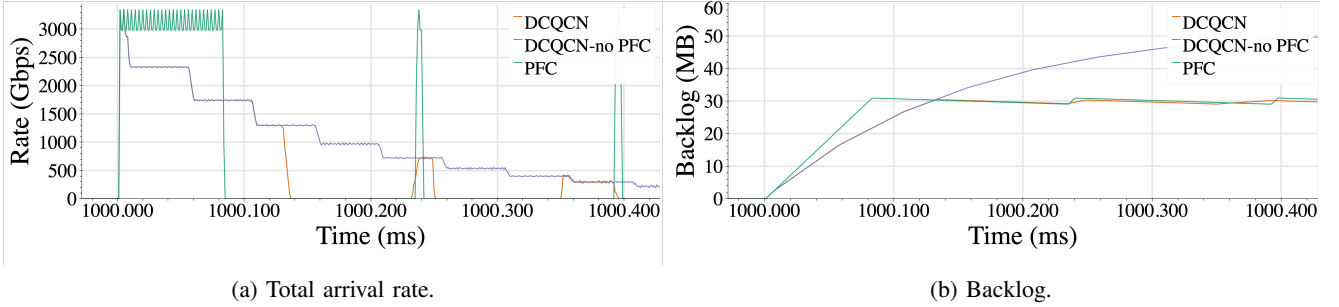


Fig. 8: Simulation of burst arrivals (400 μ s).

to the line rate of 100 Gbps. Within one millisecond, by time $t = 1001$ ms, the total traffic rate is reduced significantly and remains low for the remaining duration.

The evolution of the backlog for *DCQCN* in Figure 7b shows a large backlog for a period of time exceeding 3 ms. Initially, for the interval $[1000\text{ms}, 1000.8\text{ms}]$, the backlog follows that of *PFC*, indicating that congestion control is not effective with reducing the backlog in this time interval. After $t = 1000.8$ ms, the backlog decreases at the link rate until it is completely cleared. The backlog curve for *DCQCN-noPFC* shows that, without the aid of PFC, the backlog increases for a duration of about 800 μ s and exceeds 50 MB at its peak.

To study the early stages of the experiment in more detail, Figure 8 presents traffic rates and backlog for the initial 400 μ s. We first discuss *DCQCN-noPFC*. In Figure 8a we observe that the aggregate traffic rate with *DCQCN-noPFC* decreases in a stepwise fashion. The rate reduction in each step is proportional to the rate, which reflects the multiplicative decrease in DCQCN. The first rate reduction is observed within less than 10 μ s, at $t = 1000.01$ ms. Subsequent rate reductions occur in intervals of 50 μ s, which is due to the time gap T_{gap} between two CNPs. At $t = 1000.4$ ms, after eight rate reductions by the traffic senders, the aggregate arrivals still exceed the link capacity of the egress port to the destination. Therefore, the backlog continues to increase. The traffic rates in Figure 8a for *DCQCN*, which includes PFC, are initially identical to *DCQCN-noPFC*. At about $t = 1000.13$ ms, the PFC mechanism is triggered, which drops the traffic rate to zero.

B. Model-Based Analysis

For the model-based analysis, we consider a simplified version of DCQCN that focuses on the AIMD and ECN mechanisms. As a rate-based method, the model for DCQCN follows the analysis from §III-C. From Table II we obtain $\alpha = 5$ Mbps for the additive increase, and $\Delta\tau_{\text{inc}} = 55$ μ s for the interval between increases. Our model does not account for hyper increase phase shown in Table I. For the multiplicative

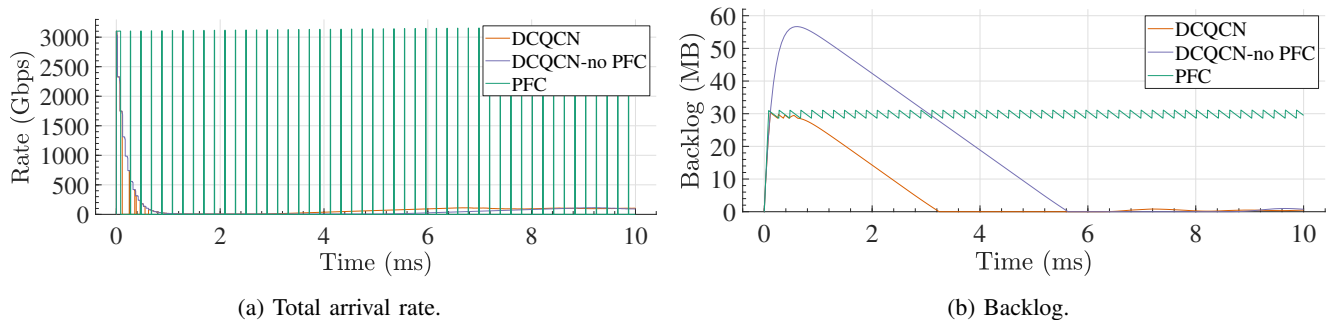


Fig. 9: Model-based characterization of burst arrivals (10 ms).

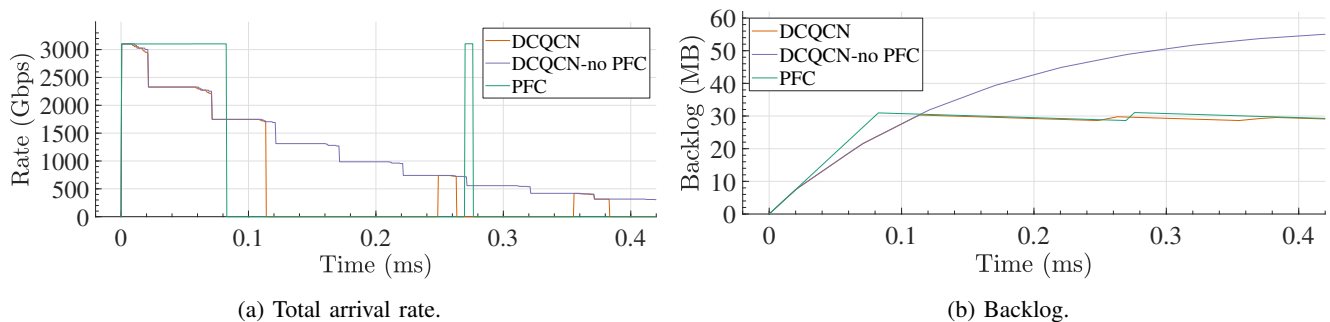


Fig. 10: Model-based characterization of burst arrivals (400 μ s).

decrease, instead of accounting for a variable factor as used in DCQCN, we always apply a constant multiplicative factor $\beta = 0.75$, which is obtained empirically from simulation experiments. For ECN and PFC, our model follows the description in §III-B. The ECN model accounts for RED with parameters given in Table II. The minimum distance between back-to-back congestion notifications is set to $\Delta\tau_{\text{ecn}} = 50 \mu\text{s}$. The PFC parameters are as described above. Since PFC prevents packet losses, retransmission timeouts only play a role in the *DCQCN-noPFC* scenario. We use a timeout value of $\tau_o = 3 \text{ ms}$ in all scenarios.

As arrival traffic, we consider simultaneous burst arrivals of 10 MB from 31 sources with rate limits set to 100 Gbps at the start of the bursts. We set the service curve of the path server to $S(t) = \max\{Ct, 0\}$ where $C = 100 \text{ Gbps}$. The feedback delay, ΔR , is set to $4 \mu\text{s}$, which corresponds to the total propagation round-trip delay.

Figures 9 and 10 present the traffic rate and backlog obtained from our model, where Figure 10 focuses on the first 400 μs . Traffic rates are computed by adding the admitted arrival functions \hat{A} of all sources and then averaging over the same time intervals as in the simulations. A comparison with the simulation results shows that the network calculus model closely tracks the behavior of both DCQCN and PFC. The – sometimes subtle – deviations are due to shortcuts in our DCQCN model. As one example, in Figure 9b we see that the backlog for DCQCN increases after an initial spike at around 7 ms. In the simulations (Figure 7b) we observe the secondary spike much earlier at around 3 ms. Since we do not consider the hyper increase phase of DCQCN in our model, the traffic rates recover more slowly. This can be observed by comparing the transmission rates. In the simulations (Figure 7a) we observe a non-linear jump to 300 Gbps at 3 ms, whereas the model (Figure 9a) shows a linear increase until the 7 ms mark, when the maximum rate of 100 Gbps is reached.

VI. RELATED WORK

The late 1990s and early 2000s were a golden era for analytical modeling of TCP congestion control, and many methods available today originate in that period. A seminal work by Kelly et al. [48] presented the first mathematical analysis of congestion control dynamics in a general network where rate allocations were formulated in economic terms as a utility optimization. This and many works that followed [49], [50], [51], [52], [19] derived stability and convergence properties of various congestion control mechanisms and TCP variants

A different analysis approach from that era describes TCP dynamics by a coupled system of differential equations [53] for tracking its transient behavior. With this, it is possible to relate congestion control to classical control theoretic closed loop systems [54], [55]. Until today, coupled differential equation systems are the prevalent method for characterizing CAA dynamics [5], [22], [23]. The above approaches do not account for the interactions between source traffic and congestion control, which is needed to study congestion control of intermittent but bursty traffic.

Network calculus is an alternative approach for studying feedback systems. Agrawal et al. [30] derived a service curve for a window flow control system with a fixed window size. Baccelli and Hong [56] expressed the feedback loop of TCP in a max-plus dioid algebra. Assuming fixed-sized packets, permanently backlogged sources, and excluding retransmissions they showed that TCP satisfies max-plus linearity.⁴ Kim and Hou [57] showed that the rate limits imposed by AIMD can be viewed as a piece-wise linear shaper. A recent study [28] applied techniques inspired by network calculus to study scenarios where CCAs fail. Specific loss scenarios are expressed in terms of constraints on arrivals and departures to create a satisfiability problem. In [28], the network is represented as a generalized token bucket, referred to as path server, which determines the available bandwidth to a traffic flow. The network model of our paper is derived from the path server model and shares many of its assumptions.

VII. CONCLUSIONS

We have developed a modular model-based approach to the analysis of CCAs that can account for bursty traffic sources. Using a path server network model, we characterized rate-based and window-based congestion control algorithms within the framework of the network calculus. By performing an analysis within time intervals where the network satisfies linearity conditions and appropriately shifting the reference coordinate system, we were able to conduct a linear analysis of an overall non-linear network. We showed that our model-based characterization can capture convergence toward fairness of a CCA. The network calculus characterization of congestion control provides an alternative tool for studying the dynamics of CCA, which can achieve a high degree of accuracy. This was demonstrated in a case study of burst transmissions in a data center network which deploy PFC and DCQCN.

⁴Max-plus and min-plus linear systems are dual to each other [31].

REFERENCES

- [1] Q. Zhang, V. Liu, H. Zeng, and A. Krishnamurthy, “High-resolution measurement of data center microbursts,” in *Proc. ACM IMC*, November 2017, pp. 78–85.
- [2] R. Kapoor, A. C. Snoeren, G. M. Voelker, and G. Porter, “Bullet trains: a study of NIC burst behavior at microsecond timescales,” in *Proc. ACM CoNEXT*, December 2013, pp. 133–138.
- [3] X. Chen, S. L. Feibish, Y. Koral, J. Rexford, and O. Rottenstreich, “Catching the microburst culprits with Snappy,” in *Proc. ACM SIGCOMM Workshop on Self-Driving Networks*, August 2018, pp. 22–28.
- [4] D. Shan, F. Ren, P. Cheng, R. Shu, and C. Guo, “Observing and mitigating micro-burst traffic in data center networks,” *IEEE/ACM Transactions on Networking*, vol. 28, no. 1, pp. 98–111, 2020.
- [5] Y. Zhu, H. Eran, D. Firestone, C. Guo, M. Lipshteyn, Y. Liron, J. Padhye, S. Raindel, M. H. Yahia, and M. Zhang, “Congestion control for large-scale RDMA deployments,” in *Proc. ACM SIGCOMM*, August 2015, pp. 523–536.
- [6] S. Bensley, D. Thaler, P. Balasubramanian, L. Eggert, and G. Judd, “Data center TCP (DCTCP): TCP congestion control for data centers,” Internet Request for Comments, RFC 8257, October 2017.
- [7] Y. Li, R. Miao, H. H. Liu, Y. Zhuang, F. Feng, L. Tang, Z. Cao, M. Zhang, F. Kelly, M. Alizadeh, and M. Yu, “HPCC: high precision congestion control,” in *Proc. ACM SIGCOMM*, August 2019, pp. 44–58.
- [8] R. Mittal, V. T. Lam, N. Dukkupati, E. Blem, H. Wassel, M. Ghobadi, A. Vahdat, Y. Wang, D. Wetherall, and D. Zats, “TIMELY: RTT-based congestion control for the datacenter,” in *Proc. ACM SIGCOMM*, October 2015, pp. 537–550.
- [9] G. Kumar, N. Dukkupati, K. Jang, H. M. G. Wassel, X. Wu, B. Montazeri, Y. Wang, K. Springborn, C. Alfeld, M. Ryan, D. Wetherall, and A. Vahdat, “Swift: delay is simple and effective for congestion control in the datacenter,” in *Proc. ACM SIGCOMM*, July 2020, pp. 514–528.
- [10] A. Mushtaq, R. Mittal, J. McCauley, M. Alizadeh, S. Ratnasamy, and S. Shenker, “Datacenter congestion control,” *ACM SIGCOMM Computer Communication Review*, vol. 49, no. 3, pp. 32–38, 2019.
- [11] S. Ketabi and Y. Ganjali, “Hierarchical congestion control (HCC): fairness and fast convergence for data centers,” in *Proc. IFIP Networking*, June 2022, pp. 1–9.
- [12] D. Shan and F. Ren, “Improving ECN marking scheme with micro-burst traffic in data center networks,” in *Proc. IEEE INFOCOM*, May 2017, pp. 1–9.
- [13] S. Yan, X. Wang, X. Zheng, Y. Xia, D. Liu, and W. Deng, “ACC: automatic ECN tuning for high-speed datacenter networks,” in *Proc. ACM SIGCOMM*, August 2021, pp. 384–397.
- [14] Infiniband Trade Association, “InfiniBand Architecture Specification, Volume 1, Release 1.2.1,” 2007, November 2007.
- [15] —, “InfiniBand Architecture Specification Release 1.2.1 Annex A17: RoCEv2,” 2014, September 2014.
- [16] K. He, E. Rozner, K. Agarwal, Y. Gu, W. Felter, J. Carter, and A. Akella, “AC/DC TCP: virtual congestion control enforcement for datacenter networks,” in *Proc. ACM SIGCOMM*, August 2016, pp. 244–257.
- [17] Y. Liu, F. L. Presti, V. Misra, D. F. Towsley, and Y. Gu, “Fluid models and solutions for large-scale IP networks,” in *Proc. ACM SIGMETRICS*, June 2003, pp. 91–101.
- [18] G. Vardoyan, C. V. Hollot, and D. Towsley, “Towards stability analysis of data transport mechanisms: a fluid model and its applications,” *IEEE/ACM Transactions on Networking*, vol. 29, no. 4, pp. 1730–1744, 2021.
- [19] R. Srikant, *The Mathematics of Internet Congestion Control*, ser. Systems & Control: Foundations & Applications. Birkhäuser Boston, 2012.
- [20] S. H. Low, F. Paganini, and J. C. Doyle, “Internet congestion control,” *IEEE Control Systems Magazine*, vol. 22, no. 1, pp. 28–43, 2002.
- [21] S. Shakkottai and R. Srikant, “How good are deterministic fluid models of internet congestion control?” in *Proc. IEEE INFOCOM*, June 2002, pp. 497–505.
- [22] M. Alizadeh, A. Javanmard, and B. Prabhakar, “Analysis of DCTCP: stability, convergence, and fairness,” in *Proc. ACM SIGMETRICS*, June 2011, pp. 73–84.
- [23] S. Scherrer, M. Legner, A. Perrig, and S. Schmid, “Model-based insights on the performance, fairness, and stability of BBR,” in *Proc. ACM IMC*, October 2022, pp. 519–537.
- [24] K. He, X. Zhang, S. Ren, and J. Sun, “Deep residual learning for image recognition,” in *Proc. IEEE Conference on Computer Vision and Pattern Recognition (CVPR)*, June 2016, pp. 770–778.
- [25] J.-Y. L. Boudec and P. Thiran, *Network calculus: a theory of deterministic queueing systems for internet*. Springer-Verlag, 2001.
- [26] C.-S. Chang, *Performance guarantees in communication networks*. Springer-Verlag, 2000.
- [27] A. Bouillard, M. Boyer, and E. L. Corronc, *Deterministic network calculus: from theory to practical implementation*. John Wiley & Sons, December 2018.
- [28] V. Arun, M. T. Arashloo, A. Saeed, M. Alizadeh, and H. Balakrishnan, “Toward formally verifying congestion control behavior,” in *Proc. ACM SIGCOMM*, August 2021, pp. 1–16.
- [29] L. S. Brakmo and L. L. Peterson, “TCP Vegas: end to end congestion avoidance on a global internet,” *IEEE Journal on Selected Areas in Communications*, vol. 13, no. 8, pp. 1465–1480, 1995.
- [30] R. Agrawal, R. L. Cruz, C. Okino, and R. Rajan, “Performance bounds for flow control protocols,” *IEEE/ACM Transactions on Networking*, vol. 7, no. 3, pp. 310–323, 1999.

- [31] J. Liebeherr, "Duality of the max-plus and min-plus network calculus," *Foundations and Trends in Networking*, vol. 11, no. 3–4, pp. 139–282, 2016.
- [32] R. Zippo, P. Nikolaus, and G. Stea, "Extending the network calculus algorithmic toolbox for ultimately pseudo-periodic functions: pseudo-inverse and composition," *Discrete Event Dynamic Systems*, vol. 33, no. 3, pp. 181–219, 2023.
- [33] K. Fall and S. Floyd, "Simulation-based comparisons of Tahoe, Reno and SACK TCP," *ACM SIGCOMM Computer Communication Review*, vol. 26, no. 3, pp. 5–21, 1996.
- [34] K. K. Ramakrishnan, S. Floyd, and D. L. Black, "The addition of explicit congestion notification (ecn) to IP," Internet Request for Comments, RFC 3168, September 2001.
- [35] S. Floyd and V. Jacobson, "Random early detection gateways for congestion avoidance," *IEEE/ACM Transactions on Networking*, vol. 1, no. 4, pp. 397–413, 1993.
- [36] IEEE, "IEEE standard for local and metropolitan area networks—media access control (MAC) bridges and virtual bridged local area networks—Amendment 17: Priority-based Flow Control," *IEEE Std 802.1Qbb*, 2011.
- [37] D.-M. Chiu and R. Jain, "Analysis of the increase and decrease algorithms for congestion avoidance in computer networks," *Computer Networks and ISDN Systems*, vol. 17, no. 1, pp. 1–14, 1989.
- [38] V. Jacobson, "Congestion avoidance and control," in *Proc. ACM SIGCOMM*, August 1988, pp. 314–329.
- [39] S. Ha, I. Rhee, and L. Xu, "CUBIC: a new TCP-friendly high-speed TCP variant," *ACM SIGOPS Operating Systems Review*, vol. 42, no. 5, pp. 64–74, 2008.
- [40] G. F. Riley and T. R. Henderson, *The ns-3 Network Simulator*. Springer Berlin Heidelberg, 2010, pp. 15–34.
- [41] C. Samios and J. K. Vernon, "Modeling the throughput of TCP Vegas," *Proc. ACM SIGMETRICS*, p. 71–81, Jun. 2003.
- [42] Nvidia Corporation. (2022) How to configure DCQCN values for ConnectX-4. (Accessed on: 2023-11-10). [Online]. Available: <https://enterprise-support.nvidia.com/s/article/howto-configure-dcqcn--roce-cc--values-for-connectx-4--linux-x>
- [43] Cisco System. (2023) Cisco Data Center Networking Blueprint for AI/ML Applications. (Accessed on: 2023-11-10). [Online]. Available: <https://www.cisco.com/c/en/us/td/docs/dcn/whitepapers/cisco-data-center-networking-blueprint-for-ai-ml-applications.html>
- [44] Juniper Networks. (2021) Data Center Quantized Congestion Notification (DCQCN). (Accessed on: 2023-11-10). [Online]. Available: <https://www.juniper.net/documentation/us/en/software/junos/traffic-mgmt-qfx/topics/topic-map/cos-qfx-series-DCQCN.html>
- [45] Huawei. (2023) CloudEngine 16800, 12800, 9800, 8800, 7800, 6800, and 5800 Series Switches Typical Configuration Examples: Configuring an Intelligent Lossless Network. (Accessed on: 2023-11-10). [Online]. Available: <https://support.huawei.com/enterprise/en/doc/EDOC1000039339/5b5d82a2/configuring-an-intelligent-lossless-network>
- [46] IEEE, "IEEE standard for local and metropolitan area networks—virtual bridged local area network—Amendment 13: Congestion Notification," *IEEE Std 802.1Qau*, 2010.
- [47] Y. Zhu, M. Ghobadi, V. Misra, and J. Padhye. (2016) NS-3 simulator for RDMA. [Online]. Available: <https://github.com/bobzhuyb/ns3-rdma>
- [48] F. P. Kelly, A. K. Maulloo, and D. K. H. Tan, "Rate control for communication networks: shadow prices, proportional fairness and stability," *Journal of the Operational Research Society*, vol. 49, no. 3, pp. 237–252, 1998.
- [49] S. H. Low and D. E. Lapsley, "Optimization flow control. I. basic algorithm and convergence," *IEEE/ACM Transactions on Networking*, vol. 7, no. 6, pp. 861–874, 1999.
- [50] S. H. Low, "A duality model of TCP and queue management algorithms," *IEEE/ACM Transactions On Networking*, vol. 11, no. 4, pp. 525–536, 2003.
- [51] S. H. Low, L. L. Peterson, and L. Wang, "Understanding TCP Vegas: a duality model," *Journal of the ACM*, vol. 49, no. 2, pp. 207–235, 2002.
- [52] S. Kunniyur and R. Srikant, "End-to-end congestion control schemes: utility functions, random losses and ECN marks," *IEEE/ACM Transactions on Networking*, vol. 11, no. 5, pp. 689–702, 2003.
- [53] V. Misra, W.-B. Gong, and D. Towsley, "Fluid-based analysis of a network of AQM routers supporting TCP flows with an application to RED," in *Proc. ACM SIGCOMM*, 2000, pp. 151–160.
- [54] C. V. Hollot, V. Misra, D. Towsley, and W.-B. Gong, "A control theoretic analysis of RED," in *Proc. IEEE INFOCOM*, 2001, pp. 1510–1519.
- [55] C. V. Hollot, V. Misra, D. Towsley, and W. Gong, "Analysis and design of controllers for AQM routers supporting TCP flows," *IEEE Transactions on Automatic Control*, vol. 47, no. 6, pp. 945–959, 2002.
- [56] F. Baccelli and D. Hong, "TCP is max-plus linear and what it tells us on its throughput," in *Proc. ACM SIGCOMM*, August 2000, pp. 219–230.
- [57] H. Kim and J. C. Hou, "Network calculus based simulation for TCP congestion control: theorems, implementation and evaluation," in *Proc. IEEE INFOCOM*, 2004, pp. 2844–2855.

APPENDIX A
ALGORITHM FOR RATE-BASED CONGESTION CONTROL

Algorithm 1 summarizes the computations for a rate-based CCA with an AIMD scheme. The algorithm takes as input an arrival function in the range $[0, t_{\text{end}}]$. The service curve of the path server is a rate function with initial rate r_o . We can distinguish five phases: (1) initial calculation of \hat{A} and D with the input parameters (steps 1–4); (2) determination of the next congestion event (steps 6–8), (3) adjustment of the rate limit based on the type of congestion event (steps 10–12 and 17–18), (4) updating the arrival and admitted arrival functions in a shifted coordinate system (steps 12–15 and 19–22), and finally (5) updating the departure function (steps 24–25). Steps (2)–(5) are repeated until no more congestion events are found.

Algorithm 1: Network calculus computation of rate-based AIMD congestion control.

Input: $A, S, \alpha, \beta, \tau_o, r_o, \Delta R, \Delta \tau_{\text{ai}}, t_{\text{end}}$
Output: D, \hat{A}

```

1  $r \leftarrow r_o$  ,  $t_{\text{TO}}^{\text{prev}} \leftarrow 0$  ,  $t_{\text{AI}} \leftarrow 0$ 
2  $S_r(t) \leftarrow \max\{rt, 0\}$ , for  $t \in [0, t_{\text{end}}]$ 
3  $\hat{A}(t) \leftarrow A \otimes S_r(t)$  , for  $t \in [0, t_{\text{end}}]$ 
4  $D(t) \leftarrow \hat{A} \otimes S(t)$  , for  $t \in [0, t_{\text{end}}]$ 
5 repeat
6    $t_{\text{AI}} \leftarrow \min\{t_{\text{AI}} + \Delta \tau_{\text{ai}}, t_{\text{end}}\}$ 
7    $t_{\text{TO}}^{\text{next}} \leftarrow \min\{t > t_{\text{TO}}^{\text{next}} \mid D(t - \Delta R) < \hat{A}(t - \tau_o)\}$ 
8    $t_{\text{event}} \leftarrow \min\{t_{\text{TO}}^{\text{next}}, t_{\text{AI}}\}$ 
9   if  $t_{\text{event}} = t_{\text{TO}}^{\text{next}}$  then
10      $t_{\text{TO}}^{\text{prev}} \leftarrow t_{\text{TO}}^{\text{next}}$ 
11      $r \leftarrow \beta r$ 
12      $S_r(t) \leftarrow \max\{rt, 0\}$ , for  $t \in [0, t_{\text{end}} - t_{\text{event}}]$ 
13      $A^{\text{rem}}(t) \leftarrow A(t + t_{\text{event}}) - D(t_{\text{event}} - \Delta R)$ , for  $t \in [0, t_{\text{end}} - t_{\text{event}}]$ 
14      $\hat{A}^{\text{rem}}(t) \leftarrow A^{\text{rem}} \otimes S_r(t)$ , for  $t \in [0, t_{\text{end}} - t_{\text{event}}]$ 
15      $\hat{A}(t) \leftarrow \hat{A}^{\text{rem}}(t - t_{\text{event}}) + D(t_{\text{event}} - \Delta R)$ , for  $t \in [t_{\text{event}}, t_{\text{end}}]$ 
16   else
17      $r \leftarrow r + \alpha$ 
18      $S_r(t) \leftarrow \max\{rt, 0\}$ , for  $t \in [0, t_{\text{end}} - t_{\text{event}}]$ 
19      $A^{\text{rem}}(t) \leftarrow A(t + t_{\text{event}}) - A(t_{\text{event}})$ , for  $t \in [0, t_{\text{end}} - t_{\text{event}}]$ 
20      $\hat{A}^{\text{rem}}(t) \leftarrow A^{\text{rem}} \otimes S_r(t)$ , for  $t \in [0, t_{\text{end}} - t_{\text{event}}]$ 
21      $\hat{A}(t) \leftarrow \hat{A}^{\text{rem}}(t - t_{\text{event}}) + A(t_{\text{event}})$ , for  $t \in [t_{\text{event}}, t_{\text{end}}]$ 
22      $\hat{A}^{\text{rem}}(t) \leftarrow \hat{A}(t + t_{\text{TO}}^{\text{prev}}) - D(t_{\text{TO}}^{\text{prev}})$ , for  $t \in [0, t_{\text{end}} - t_{\text{TO}}^{\text{prev}}]$ 
23   end
24    $D^{\text{rem}}(t) \leftarrow \hat{A}^{\text{rem}} \otimes S(t)$ , for  $t \in [0, t_{\text{end}} - t_{\text{TO}}^{\text{prev}}]$ 
25    $D(t) \leftarrow D^{\text{rem}}(t - t_{\text{TO}}^{\text{prev}}) + D(t_{\text{TO}}^{\text{prev}} - \Delta R)$ , for  $t \in [t_{\text{TO}}^{\text{prev}}, t_{\text{end}}]$ 
26 until  $t_{\text{event}} \geq t_{\text{end}}$ 

```

APPENDIX B

ALGORITHM FOR WINDOW-BASED CONGESTION CONTROL

Algorithm 2 presents the computations for a window-based flow control, which is similar to TCP Tahoe, for an arrival function $A(t)$ for $t \leq t_{\text{end}}$. Like Algorithm 1, the algorithm updates \hat{A} and D in iterations depending on encountered congestion events. Steps 11–14 and steps 18–20 show the updates of \hat{A} after an update of the window size.

Algorithm 2: Network calculus computation of window-based AIMD congestion control.

Input: $A, S, \alpha, \beta, \tau_o, \Delta R, W_o, w_{tho}$ (initial slow start threshold), t_{end}

Output: D, \hat{A}

```

1  $W \leftarrow W_o, t_{\text{TO}}^{\text{prev}} \leftarrow 0$ 
2  $w_{th} \leftarrow w_{tho}$ 
3  $S_W(t) \leftarrow W$ , for  $t \in [0, t_{\text{end}}]$ 
4  $\hat{A}(t) \leftarrow \hat{A} \otimes S_W(t)$ , for  $t \in [0, t_{\text{end}}]$ 
5  $D(t) \leftarrow \hat{A} \otimes S(t)$ , for  $t \in [0, t_{\text{end}}]$ 
6 repeat
7    $t_W \leftarrow \min \{t \mid D(t - \Delta R) > W\}$ 
8    $t_{\text{TO}}^{\text{next}} \leftarrow \min \{t \mid D(t - \Delta R) < \hat{A}(t - \tau_o)\}$ 
9    $t_{\text{event}} \leftarrow \min \{t_{\text{TO}}^{\text{next}}, t_W\}$ 
10  if  $t_{\text{event}} = t_{\text{TO}}^{\text{next}}$  then
11     $t_{\text{TO}}^{\text{prev}} \leftarrow t_{\text{TO}}^{\text{next}}$ 
12     $w_{th} \leftarrow \beta W$ 
13     $W \leftarrow W_o$ 
14     $A^{\text{rem}}(t) \leftarrow A(t + t_{\text{event}}) - D(t_{\text{event}} - \Delta R)$ , for  $t \in [0, t_{\text{end}} - t_{\text{event}}]$ 
15     $S_W(t) \leftarrow W$ , for  $t \in [0, t_{\text{end}} - t_{\text{event}}]$ 
16     $\hat{A}^{\text{rem}}(t) \leftarrow A^{\text{rem}} \otimes S_W(t)$ , for  $t \in [0, t_{\text{end}} - t_{\text{event}}]$ 
17     $\hat{A}(t) \leftarrow \hat{A}^{\text{rem}}(t - t_{\text{event}}) + D(t_{\text{event}} - \Delta R)$ , for  $t \in [t_{\text{event}}, t_{\text{end}}]$ 
18  else
19    Update  $W$  according to Eq. (7)
20     $A^{\text{rem}}(t) \leftarrow A(t + t_{\text{event}}) - A(t_{\text{event}})$ , for  $t \in [0, t_{\text{end}} - t_{\text{event}}]$ 
21     $S_W(t) \leftarrow W$ , for  $t \in [0, t_{\text{end}} - t_{\text{event}}]$ 
22     $\hat{A}^{\text{rem}}(t) \leftarrow A^{\text{rem}} \otimes S_W(t)$ , for  $t \in [0, t_{\text{end}} - t_{\text{event}}]$ 
23     $\hat{A}(t) \leftarrow \hat{A}^{\text{rem}}(t - t_{\text{event}}) + A(t_{\text{event}})$ , for  $t \in [t_{\text{event}}, t_{\text{end}}]$ 
24     $\hat{A}^{\text{rem}}(t) \leftarrow \hat{A}(t + t_{\text{TO}}^{\text{prev}}) - D(t_{\text{TO}}^{\text{prev}})$ , for  $t \in [0, t_{\text{end}} - t_{\text{TO}}^{\text{prev}}]$ 
25  end
26   $D^{\text{rem}} \leftarrow \hat{A}^{\text{rem}} \otimes S(t)$ , for  $t \in [0, t_{\text{end}} - t_{\text{TO}}^{\text{prev}}]$ 
27   $D(t) \leftarrow D^{\text{rem}}(t - t_{\text{TO}}^{\text{prev}}) + D(t_{\text{TO}}^{\text{prev}} - \Delta R)$ , for  $t \in [t_{\text{TO}}^{\text{prev}}, t_{\text{end}}]$ 
28 until  $t_{\text{event}} \geq t_{\text{end}}$ 

```

APPENDIX C
ALGORITHM FOR TCP VEGAS

Algorithm 3 summarizes the computations for TCP Vegas. Whenever the current RTT estimate $minRTT$ is updated (lines 6-7), we update W (lines 8-25), along with \hat{A} and D (lines 26-30). The algorithm does not account for timeouts and retransmissions. We indicate slow start using $Flag_{slowstart}$ and $Flag_{skip}$ ensures updates only occur every other RTT in this phase. We use w_{low} and w_{high} to denote the α and β thresholds in [29], [41], respectively. The definitions for γ , $baseRTT$ and $diff$ are identical to [29], [41].

Algorithm 3: Network calculus computation of TCP Vegas without timeouts.

Input: $A, S, \Delta R, W_o, t_{end}, I_{max}, w_{low}, w_{high}, \gamma$
Output: D, \hat{A}

```

1  $W \leftarrow W_o$ ,  $t_{event} \leftarrow 0$ ,  $Flag_{slowstart} \leftarrow 1$ ,  $Flag_{skip} \leftarrow 0$ 
2  $baseRTT \leftarrow \Delta R$ ,  $minRTT \leftarrow \Delta R$ 
3  $\hat{A}(t) \leftarrow \hat{A} \otimes S_W(t)$ , for  $t \in [0, t_{end}]$ 
4  $D(t) \leftarrow \hat{A} \otimes S(t)$ , for  $t \in [0, t_{end}]$ 
5 repeat
6    $t_{event} \leftarrow t_{event} + minRTT$ 
7    $minRTT \leftarrow RTT(t_{event})$  according to Eq. (1)
8    $diff \leftarrow baseRTT \cdot (\frac{W}{baseRTT} - \frac{W}{minRTT})$ 
9   if  $Flag_{slowstart} = 1$  then
10    if  $diff > \gamma$  then
11       $W \leftarrow W \cdot \frac{baseRTT}{minRTT}$ 
12       $Flag_{slowstart} \leftarrow 0$ 
13    else
14      if  $Flag_{skip} = 0$  then
15         $W \leftarrow 2 \cdot W$ 
16      end
17       $Flag_{skip} \leftarrow (1 + Flag_{skip}) \bmod 2$ 
18    end
19  else
20    if  $diff < w_{low}$  then
21       $W \leftarrow W + I_{max}$ 
22    else if  $diff > w_{high}$  then
23       $W \leftarrow W - I_{max}$ 
24    end
25  end
26   $A^{rem}(t) \leftarrow A(t + t_{event}) - A(t_{event})$ , for  $t \in [0, t_{end} - t_{event}]$ 
27   $\hat{W}(t) \leftarrow \max \left\{ 0, W - (\hat{A}(t_{event}) - D(t + t_{event} - \Delta R)) \right\}$ , for  $t \in [0, t_{end} - t_{event}]$ 
28   $\hat{A}^{rem}(t) \leftarrow \min \left\{ A^{rem}(t), \hat{W}(t) \right\}$ , for  $t \in [0, t_{end} - t_{event}]$ 
29   $\hat{A}(t) \leftarrow \hat{A}^{rem}(t - t_{event}) + A(t_{event})$ , for  $t \in [t_{event}, t_{end}]$ 
30   $D(t) \leftarrow \hat{A} \otimes S(t)$ , for  $t \in [0, t_{end}]$ 
31 until  $t_{event} \geq t_{end}$ 

```

APPENDIX D

PROOFS

A. Proof of Lemma 1

To show Eq. (9), select a flow $i \in \mathcal{N}$ and an interval $[t', t]$ with $\hat{A}_i(t') < D_i(t)$. From the FIFO property, we can conclude that every flow $j \in X$ satisfies $\hat{A}_j(t') \leq D_j(t)$. Summing up over all flows in X yields

$$\sum_{j \in X} \hat{A}_j(t') \leq \sum_{j \in X} D_j(t).$$

For Eq. (10), we prove its converse by selecting a flow $i \in \mathcal{N}$ and an interval $[t', t]$ with $\hat{A}_i(t') > D_i(t)$. Then, due to the FIFO property, every flow $j \in X$ satisfies $\hat{A}_j(t') \geq D_j(t)$. In this case, summing up over all flows in X yields

$$\sum_{j \in X} \hat{A}_j(t') \geq \sum_{j \in X} D_j(t).$$

□

B. Proof of Lemma 2

Consider a set of flows that satisfies Eq. (11). Suppose that there is some flow $i \in X$ where $\hat{A}_i(t') < D_i(t)$. Due to the FIFO property, it holds that every flow $j \in X$ satisfies $\hat{A}_j(t') \leq D_j(t)$. Summing up over all flows in X yields

$$\sum_{j \in X} \hat{A}_j(t') < \sum_{j \in X} D_j(t),$$

which contradicts Eq. (11). So every flow $i \in X$ satisfies $\hat{A}_i(t') \geq D_i(t)$.

Similarly, suppose that some flow $i \in X$ satisfies $\hat{A}_i(t') > D_i(t)$. Due to the FIFO property, every other flow $j \in X$ satisfies $\hat{A}_j(t') \geq D_j(t)$. Summing up over all flows in X yields

$$\sum_{j \in X} \hat{A}_j(t') < \sum_{j \in X} D_j(t),$$

which contradicts Eq. (11), and so $\hat{A}_i(t') = D_i(t)$ for all $i \in X$.

□

C. Proof of Theorem 1

The proof uses a property of the upper pseudo-inverse [31, p. 66, (P4)], which states that every left-continuous function F satisfies for every $y \in \mathbb{R}$,

$$F(F^\uparrow(y)) \leq y < F(F^\uparrow(y) + \varepsilon).$$

Setting $F = \hat{A}$ and $y = D(t)$, we obtain

$$\hat{A}(\hat{A}^\uparrow(D(t))) \leq D(t) < \hat{A}(\hat{A}^\uparrow(D(t)) + \varepsilon).$$

We then apply Lemma 1 to both inequalities in the above equation. For the right inequality, we set $X = \mathcal{N}$ and $t' = \hat{A}^\uparrow(D(t)) + \varepsilon$ to the converse of Eq. (9) to obtain

$$D_i(t) < \hat{A}_i(\hat{A}^\uparrow(D(t)) + \varepsilon).$$

For the left inequality, we split it into two cases. If $\hat{A}(\hat{A}^\uparrow(D(t))) < D(t)$, we apply Eq. (10) with $X = \mathcal{N}$ and $t' = \hat{A}^\uparrow(D(t))$ to arrive at

$$\hat{A}_i(\hat{A}^\uparrow(D(t))) \leq D_i(t). \tag{13}$$

Otherwise, $\hat{A}(\hat{A}^\uparrow(D(t))) = D(t)$, and we can apply Lemma 2 to arrive at Eq. (13).

□